LIMNOLOGY and OCEANOGRAPHY

ASLO

Limnol. Oceanogr. 9999, 2022, 1–15

doi: 10.1002/lno.12207

Respiration regimes in rivers: Partitioning source-specific respiration from metabolism time series

Enrico Bertuzzo,[1*] **Erin R. Hotchkiss**,[2] **Alba Argerich**,[3] **John S. Kominoski**,[4] **Diana Oviedo-Vargas**,[5] **Philip Savoy**,[6] **Rachel Scarlett**,[7] **Daniel von Schiller**,[8] **James B. Heffernan**[9*]

[1]Department of Environmental Sciences, Informatics and Statistics, University of Venice Ca' Foscari, Venice, Italy
[2]Department of Biological Sciences, Virginia Tech, Blacksburg, Virginia
[3]School of Natural Resources, University of Missouri, Columbia, Missouri
[4]Institute of Environment and Department of Biological Sciences, Florida International University, Miami, Florida
[5]Stroud Water Research Center, Avondale, Pennsylvania
[6]Department of Biology, Duke University, Durham, North Carolina
[7]Department of Agricultural and Biological Engineering, Purdue University, West Lafayette, Indiana
[8]Department of Evolutionary Biology, Ecology and Environmental Sciences, Institute for Water Research (IdRA), University of Barcelona, Barcelona, Spain
[9]Nicholas School of the Environment, Duke University, Durham, North Carolina

Abstract

Respiration in streams is controlled by the timing, magnitude, and quality of organic matter (OM) inputs from internal primary production and external fluxes. Here, we estimated the contribution of different OM sources to seasonal, annual, and event-driven characteristics of whole-stream ecosystem respiration (ER) using an inverse modeling framework that accounts for possible time-lags between OM inputs and respiration. We modeled site-specific, dynamic OM stocks contributing to ER: autochthonous OM from gross primary production (GPP); allochthonous OM delivered during flow events; and seasonal pulses of leaf litter. OM stored in the sediment and dissolved organic matter (DOM) transported during baseflow were modeled as a stable stock contributing to baseline respiration. We applied this modeling framework to five streams with different catchment size, climate, and canopy cover, where multi-year time series of ER and environmental variables were available. Overall, the model explained between 53% and 74% of observed ER dynamics. Respiration of autochthonous OM tracked seasonal peaks in GPP in spring or summer. Increases in ER were often associated with high-flow events. Respiration associated with litter inputs was larger in smaller streams. Time lags between leaf inputs and respiration were longer than for other OM sources, likely due to lower biological reactivity. Model estimates of source-specific ER and OM stocks compared well with existing measures of OM stocks, inputs, and respiration or decomposition. Our modeling approach has the potential to expand the scale of comparative analyses of OM dynamics within and among freshwater ecosystems.

*Correspondence: enrico.bertuzzo@unive.it; james.heffernan@duke.edu

Additional Supporting Information may be found in the online version of this article.

Author Contribution Statement: All authors contributed to the initial conception of the study. E.R.H., P.S., and J.B.H. contributed to the acquisition and processing of the data. A.A., J.S.K., D.O.V., R.S., and D.v.S. contributed to the acquisition and processing of literature values for model comparison. E.B. carried out the analysis. E.B., E.R.H., D.O.V., D.v.S., and J.B.H. drafted the 1st version of the manuscript. All authors contributed to writing the final version of the manuscript.

Organic matter (OM) is a fundamental energy and nutrient source supporting aquatic ecosystem structure and functioning (Tank et al. 2010). Dissolved organic matter (DOM) and particulate organic matter (POM) enter streams and rivers from many sources and are transported and processed throughout river networks (Tank et al. 2010). The metabolism of OM during transit influences many important ecological functions of river networks. The balance of OM inputs, storage, transformation, metabolism, and transport affects OM delivery to downstream rivers, lakes, estuaries, and oceans (Prairie and Cole 2009), and fluxes of carbon dioxide and other greenhouse gases to the atmosphere (Battin et al. 2008). Aerobic respiration of OM is a major control of dissolved oxygen in river networks. When

respiration rates exceed oxygen supply via water-atmosphere exchange, rivers can become hypoxic, stressing aquatic organisms (Mallin et al. 2006). Dissolved oxygen concentrations can also shape the rates and dynamics of anaerobic processes that transform nutrients and produce greenhouse gases (Mulholland et al. 2008; Stanley et al. 2016).

The characterization of stream metabolic regimes links the magnitude, variability and timing of ecosystem respiration (ER) and gross primary production (GPP) to the proximate and ultimate ecosystem controls that shape these dynamics (Bernhardt et al. 2018). At the ecosystem level, GPP represents the total amount of carbon fixed by photosynthetic and chemosynthetic organisms, while ER quantifies the mineralization of organic carbon by autotrophic and heterotrophic organisms. The autotrophic component of these regimes (Bernhardt et al. 2018; Koenig et al. 2019; Savoy et al. 2019) reflects how GPP and biomass accrual primarily respond to seasonal patterns of light, temperature, flow variation and nutrient availability. The dynamics of ER partially track patterns in GPP, through autotrophic respiration and heterotrophic respiration of exudates of OM produced by autotrophs, but also reflect the dynamics of heterotrophic activity that respond to external OM inputs (Williams and del Giorgio 2005). ER regimes, the dynamic sum of respiration of OM derived from different sources, are therefore likely to be much more spatially and temporally complex than primary productivity regimes. Indeed, heterotrophic respiration may be fueled by decomposition of allochthonous OM coming from adjacent terrestrial ecosystems. Such OM could enter the stream directly (e.g., through litterfall) or by hydrologic transport of POM or DOM. Each of these OM stocks that fuel respiration has a distinct phenology, transport timescale, residence time within a stream reach, and decomposition dynamics. Biological reactivity of OM derived from different sources can potentially vary in time and depend on environmental conditions. Local abiotic and biotic conditions influence spatiotemporal patterns of OM metabolism, storage, and downstream transport. Predicting changes to ER regimes in response to global and local environmental changes requires empirical and theoretical understanding of how the timing and magnitude of OM inputs are linked to respiratory losses (Rosemond et al. 2015; Follstad Shah et al. 2017; Kominoski et al. 2018).

The rapid expansion of continuous, long-term solute records is transforming our understanding of catchment hydrology and aquatic ecosystems (Rode et al. 2016; Bernhardt et al. 2018). In isolation, such records can illustrate the timescales of variability in solute concentration and provide information about transport processes. However, quantitative integration of several time series is often necessary to estimate rates of hydrologic and biogeochemical processes. These include methods for partitioning metabolic and physical processes from oxygen time series (Holtgrieve et al. 2010; Grace et al. 2015; Appling et al. 2018), for the estimation of nutrient transformations from concurrent observations of nutrient concentrations and metabolic rates (Cohen et al. 2013; Rode et al. 2016; Kominoski et al. 2018), and for linking metabolism with nutrient and other ecosystem dynamics (Heffernan and Cohen 2010; Cohen et al. 2013; O'Donnell and Hotchkiss 2019). The shared insight of these approaches is that continuous observation allows for extraction of novel information because of the distinctive timescales of processes (e.g., photosynthesis and gas exchange, autotrophic assimilation and denitrification) and their differential relationships with environmental forcing.

Here, our objective was to advance the mechanistic understanding of how different OM sources drive whole-stream respiration dynamics. Informed by decades of studies of stream OM dynamics (Tank et al. 2010; Bernhardt et al. 2018), we developed an inverse modeling approach that combines daily estimates of GPP and ER with concurrent measures of (or proxies for) OM inputs. The model uses OM input proxies and lagged transfer functions to drive accumulation and respiration of dissolved, fine particulate, coarse particulate, and autotroph-associated OM stocks. These dynamic stocks contribute to overall ER via independent and potentially distinct respiration rates and temperature sensitivities. We applied this model to metabolic time series from five streams from a wide variety of climatic and geologic settings and a range of ecosystem sizes to assess how ER variation can be explained by differences in (1) the timing and magnitude of multiple OM inputs to streams; (2) the residence time and biological reactivity of OM derived from different sources; and (3) the dynamics of temperature and the potentially different temperature sensitivities of respiration of source-specific OM stocks. For instance, we predicted that the dominant contribution of terrestrial OM to stream ER would gradually be replaced by that of autochthonous aquatic production as channel width increases (Hotchkiss et al. 2015).

Methods

Model

To develop our model, we defined four main possible stocks of OM that can be respired in a given stream reach:

- A long-term OM stock contained in the streambed sediment or carried by the baseflow in the form of DOM or POM, whose respiration is solely controlled by water temperature T. It is assumed that this stock, C_B ($M L^{-2}$), is possibly changing only at time scales longer than those analyzed herein (up to 10 yr) and therefore it is considered constant for this exercise.
- Stock of terrestrial-derived OM that enters directly into the stream, for example, through leaf-fall, C_{LF} ($M L^{-2}$).
- OM derived from autochthonous (i.e., produced within the stream ecosystem) gross primary production, C_{GPP} ($M L^{-2}$). This OM stock includes autochthonous OM that will be respired by heterotrophs as well as OM that will be respired directly by the autotrophs themselves.
- OM related to stream discharge, C_Q ($M L^{-2}$). This stock can be primarily thought of as an allochthonous energy resource coming from adjacent terrestrial ecosystems to the

stream via hydrologic transport in the form of both POM and DOM.

To varying degrees, these stocks represent one or a few distinct pathways for respiration of OM in a stream or river. Our modeling approach quantitatively links OM stocks to specific drivers or pathways, which in some cases (litterfall, GPP) also correspond to relatively specific OM sources. However, other components (e.g., flow-associated and long-term OM stock) likely integrate OM derived from multiple sources and pathways (e.g., soil OM, litter leachate, buried or mobilized algal material). As such, our model provides insight into the sources of OM that fuel respiration, but does not neatly separate contributions of ultimate sources of OM in a strict biochemical sense.

To understand the mechanics of our model, let us first focus on a single, generic carbon stock $C(t)$. Its change over time depends on the balance between input, $I(t)$ (M L^{-2} T^{-1}), and output fluxes. The output fluxes can be further subdivided into ER, $\mathrm{ER}(t)$ (M L^{-2} T^{-1}), and nonrespiratory losses, $L(t)$ (M L^{-2} T^{-1}) (e.g., export):

$$\frac{dC(t)}{dt} = I(t) - \mathrm{ER}(t) - L(t). \tag{1}$$

Further assuming that the process is linear (i.e., output fluxes are proportional to the stock), Eq. 1 reduces to

$$\frac{dC(t)}{dt} = kP(t) - rC(t) - lC(t), \tag{2}$$

where r (T^{-1}) and l (T^{-1}) are the respiration and nonrespiratory loss rates, respectively. The input $I(t)$ is further assumed to be proportional, via the parameter k, to a measured proxy $P(t)$. In the following, proxies of OM input $P(t)$ will be: estimates of leaf litterfall $\mathrm{LF}(t)$, gross primary production $\mathrm{GPP}(t)$, and discharge $Q(t)$. The analytical solution for the stock $C(t)$, and in turn for the ER, $\mathrm{ER}(t) = rC(t)$, can be obtained from Eq. 2 using the general solution for linear, 1st-order ordinary differential equations as:

$$\mathrm{ER}(t) = rC(t) = rk\int_0^\infty P(t-t')e^{-(r+l)t'}dt'. \tag{3}$$

Equation 3 highlights how the respiration regime depends on three crucial parameters: k, r, and l. The proposed approach aims to estimate k, r, and l based on the observation of ER time series. However, these three parameters appear in groups (rk and $(r+l)$) that prevent the estimation of all three individually. Indeed, infinite combinations of the three parameters can result in the same pair of values for the two parameter groups (i.e., it is a system with three unknowns and only two equations). We therefore aggregated the parameters in two groups and obtained the following formulation:

$$\begin{aligned}\mathrm{ER}(t) &= rk\int_0^\infty P(t-t')e^{-(r+l)t'}dt' \\ &= \frac{r}{r+l}k\int_0^\infty P(t-t')\,(r+l)e^{-(r+l)t'}dt' \\ &= \beta\int_0^\infty P(t-t')\frac{e^{-t'/\tau}}{\tau}dt' = \beta P(t) * f_{\exp}(t;\tau).\end{aligned} \tag{4}$$

We thus defined two aggregated parameters β and τ that can potentially be estimated by measuring the time series of both the proxy of the input $P(t)$ and the respiration $\mathrm{ER}(t)$. $\beta = kr/(r+l)$ depends on all three parameters, whereas $\tau = 1/(r+l)$ on the respiration and non-respiratory loss rates, r and l. Note that the ratio $r/(r+l)$ represents the fraction of input that is eventually respired. This particular formulation allows writing the respiration time series as the convolution integral (symbol $*$) between the time series of the OM inputs that are eventually respired, $\beta P(t)$, and an exponential probability density function (PDF) with mean value equal to τ, $f_{\exp}(t;\tau)$. According to this formulation, the respiration at time t, $\mathrm{ER}(t)$, can be intuitively seen as the weighted sum (i.e., the integral) of the respiration of previous inputs ($\beta P(t-t')$), where the weights $(\exp(t'/\tau)dt'/\tau)$ represent the fraction of the input entered at time $(t-t')$ that is respired at time t. The exponential PDF is thus the distribution of the lag

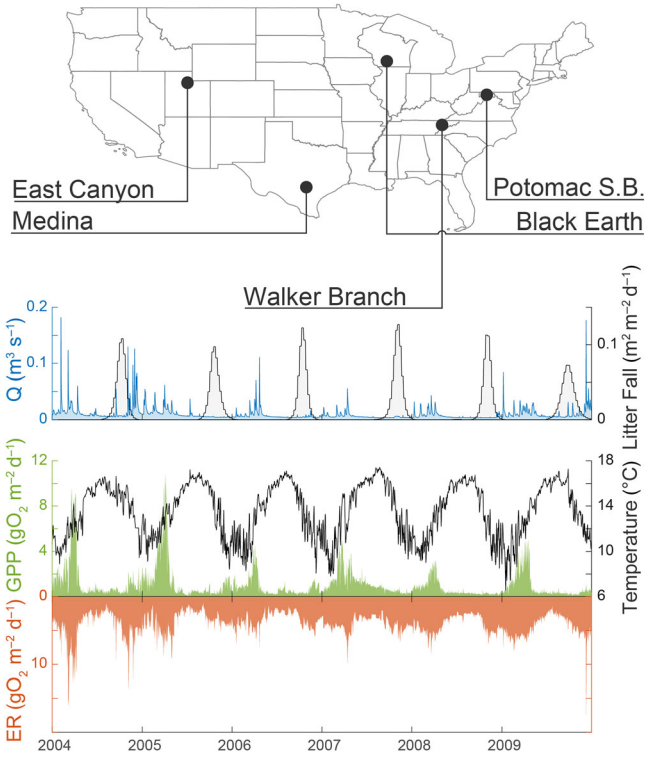

Fig. 1. Map of the conterminous Unites States with the location of the five river reaches selected as case studies for our model, and time series of Walker Branch data (bottom panel) reported as an illustrative example. Data for the remaining four sites are reported in the Supporting Information (Figs. S5, S9, S13, and S17).

between input and respiration, and τ can be interpreted as the average lag.

We further assumed that the respiration rate could be temperature dependent according to the temperature sensitivity parameter θ. The respiration of OM stock $C(t)$ is thus:

$$\mathrm{ER}(t) = \beta\theta^{T(t)-20}\int_0^\infty P(t-t')\frac{e^{-t'/\tau}}{\tau}dt, \tag{5}$$

where $T(t)$ is the water temperature in Celsius degrees at time t. Note that when the respiration rate changes with time, the analytical derivation is slightly different, but the final formulation (Eq. 5) can still be considered an effective approximation (*see* Supporting Information Appendix).

The proposed model therefore describes whole-ER at time t as the sum of the respiration of the four OM stocks:

$$\mathrm{ER}(t) = \mathrm{ER_B}(t) + \mathrm{ER_{LF}}(t) + \mathrm{ER_{GPP}}(t) + \mathrm{ER_Q}(t), \tag{6}$$

where $\mathrm{ER_B}(t)$ refers to the baseline respiration of the long-term OM stock C_B. The latter is considered constant and therefore its respiration depends only on temperature. For the remaining three components, we applied the rationale described above. The model thus finally reads:

$$\begin{aligned}\mathrm{ER}(t) = {} & \mathrm{ER_{B,20}}\theta_B^{T(t)-20} \\ & + \beta_{LF}\theta_{LF}^{T(t)-20}\int_0^\infty \mathrm{LF}(t-t')\frac{e^{-t'/\tau_{LF}}}{\tau_{LF}}dt' \\ & + \beta_{GPP}\theta_{GPP}^{T(t)-20}\int_0^\infty \mathrm{GPP}(t-t')\frac{e^{-t'/\tau_{GPP}}}{\tau_{GPP}}dt' \\ & + \beta_Q\theta_Q^{T(t)-20}\int_0^\infty Q(t-t')^{\alpha_Q}\frac{e^{-t'/\tau_Q}}{\tau_Q}dt' + \\ & + u(t),\end{aligned} \tag{7}$$

where $\mathrm{ER_{B,20}}$ is the baseline respiration at 20°C. Each dynamic OM stock is characterized by its specific β and τ parameters. We assumed that respiration temperature sensitivities could potentially be different for the different OM stocks given predicted differences in OM reactivity. OM input related to discharge is modeled as a power-law function of streamflow, that is, $Q(t)^{\alpha_Q}$. Such formulation aims at reproducing the experimental evidence of a power-law relationship between streamflow discharge and DOM concentration (Raymond and Saiers 2010; Fasching et al. 2016). To avoid the dependence of the dimension of β_Q on the parameter α_Q, we normalized discharge time series by their average value.

The term $u(t)$ in Eq. 7 represents the error term. As the first simulations indicated autocorrelated residuals, we decided to model $u(t)$ as an auto-regressive error of the form

$$u(t) = \rho\, u(t-dt) + \epsilon_t, \tag{8}$$

where $\epsilon_t = \mathcal{N}(0, \sigma_\varepsilon^2)$ is an independent, identically distributed normal variable with standard deviation equal to σ_ϵ and ρ is the autocorrelation coefficient of the error term at the dt time scale.

Conceptualizing the terms of Eq. 7 as the convolution between the input of OM that is eventually respired and the probability distribution of the lag between input and respiration allows considering a set of processes potentially more complex than those explicitly accounted for in Eq. 1, including, for example, more highly resolved transport pathways. For instance, the delay between leaf-fall in the catchment, measured by the proxy $\mathrm{LF}(t)$, and the moment in which this OM enters the stream reach could be seen as a series of transport events or pathways, for example, overland movement followed by fluvial transport from near or far upstream reaches. The net effect of these processes is a modification of the lag distribution. Our model takes a parsimonious approach based on an exponential distribution that effectively captures the mean lag, while allowing for and potentially pointing to future extensions that more precisely address specific transport processes with more complex probability distributions.

Case studies

We selected five streams as case studies for the application of the model (Fig. 1). Overall, the five case studies span a wide

Table 1. Characteristics of the five case study stream reaches.

	Walker Branch	Black Earth	East Canyon	Medina	Potomac
USGS code	—	05406457	10133800	08181500	01608500
Latitude (°)	35.9588	43.1097	40.7596	29.2641	39.4470
Longitude (°)	−84.9587	−89.6408	−111.5640	−98.4908	−78.6541
Elevation (m asl)	272	268	1902	134	171
Drainage area (km^2)	0.4	29.5	152.7	3366.9	3793.7
Mean discharge ($m^3\ s^{-1}$)	0.01	0.39	1.01	4.00	35.66
Mean water temperature (°C)	13.6	10.5	9.0	23.9	14.6
Mean leaf fall ($m^2\ m^{-2}\ yr^{-1}$)	4.6	2.1	1.7	1.9	4.6
Mean GPP (g $O_2\ m^{-2}\ yr^{-1}$)	375	1289	1365	789	1520
Mean ER (g $O_2\ m^{-2}\ yr^{-1}$)	1458	2261	1203	1559	1162

range of climatic conditions and catchment sizes: one small headwater (Walker Branch, 0.4 km^2), two catchments of intermediate size (Black Earth Creek, 30 km^2, East Canyon Creek, 153 km^2) and two large river basins (Medina River, 3367 km^2, Potomac South Branch, 3794 km^2). Table 1 summarizes the characteristics of all sites. Mean discharge, and in turn channel width according to well-established geomorphic relations (Leopold and Maddock 1953), increased with catchments size (Table 1). Therefore, analyzing results across catchment sizes allowed us to investigate also how the dominant controls on ER shifted with increasing channel width. We selected the five case study streams using the criterion of having at least four consecutive years during which all environmental variables were available. Data from four of our sites were obtained from a published dataset of stream metabolism estimates produced as part of the USGS Powell Center working group on stream metabolism (Appling et al. 2018), StreamPULSE (https://data.streampulse.org). Moreover, an updated metabolism dataset was obtained for the Walker Branch study site (Roberts et al. 2007; Roberts and Mulholland 2007).

Time series of mean daily water temperature T, mean daily discharge Q, and daily estimates of GPP and ER were taken from their respective datasets. Several preprocessing steps were performed on these datasets prior to use. We note that because we are using existing metabolism time-series datasets, methods differed between Walker Branch and the four other streams. All negative estimates of GPP and positive estimates of ER were set to not available (NA) prior to any preprocessing. Gaps in the time series for all sites except Walker Branch were filled by fitting a generalized additive model with both seasonal and trend components to each site-year of data using the mgcv package (Wood 2006) in R (R Core Team 2017). The fitted model was then used to fill in missing values which amounted to 0.2% for Black Earth, 7% for East Canyon, 8% for Medina, and 7% for Potomac. In addition, we used MODIS 8-d 500 m composite Leaf Area Index (LAI) data (MCD15A2h) (Myneni et al. 2015) to represent changes in riparian canopy status. Time series of LAI were downloaded using the Application for Extracting and Exploring Analysis Ready Samples (AppEEARS) web service (https://lpdaacsvc.cr.usgs.gov/appeears/). Noise reduction and smoothing of LAI data was performed using TIMESAT (Jönsson and Eklundh 2004; Eklundh and Jönsson 2015) and then a final set of daily LAI data was created by linearly interpolating missing values.

Finally, we further estimated a proxy of leaf litter flux as the magnitude of the (negative) time derivative of LAI when LAI decreased and assigned a value of 0 to stream leaf litter when LAI increased. This derivation implicitly assumes that leaf growth and fall are temporally separated so that the negative variation of LAI is solely due to leaf fall.

Parameter estimation

The proposed model (Eq. 7) has a total of 14 parameters (*see* Table 2) that were estimated in a Bayesian framework. Specifically, we sampled the parameter posterior distribution using the $DREAM_{zs}$ (Ter Braak and Vrugt 2008) implementation of the Markov Chain Monte Carlo algorithm. We used uniform marginal prior distributions (ranges in Table 2) for all parameters but the θ temperature sensitivity parameters, for which prior information is available. Specifically, for the θ parameters we set a Gaussian marginal prior with mean and standard deviation equal to 1.08 and 0.02, respectively. When expressed in terms of activation energy, such values correspond to approximately 0.53 and 0.12 eV K^{-1} (*see* Gillooly et al. 2001; Acuña et al. 2008). Instead of estimating the initial conditions for the three OM stocks in each stream (C_{LF}, C_{GPP}, and C_Q), we ran a 2-yr long model spin-up period forced with synthetic data obtained by replicating the 1st 2 yr of observations. The model was run at a daily timestep to match the frequency of daily ER estimates. Finally, we sampled 10^4 parameter sets from the posterior distribution and evaluated the different terms of Eq. 7 in order to derive the probability distribution of the contribution of the four main possible stocks of OM to ER.

Comparison with literature values

To assess the plausibility of the model results, we compared modeled respiration of different OM stocks to empirical values. As detailed above, the observation of the time series of respiration and of proxies of OM inputs alone does not allow the individual estimation of the respiration and non-respiratory loss rates, r and l, and of the parameter k, but just of the combined parameters β and τ. Therefore, also the OM stocks cannot be quantified from the model results (*see* from Eq. 3 how $C(t)$ depends on the values of k and $(r+l)$). The same conclusion can be intuitively achieved noting that the same respiration flux (dimension: carbon mass per unit area and time [M L^{-2} T^{-1}]) can be obtained by different pairs of respiration rate (dimension: inverse of time [T^{-1}]) and carbon stock (dimension: carbon mass per unit area [M L^{-2}]) which have the same product. We therefore first compiled literature information on empirical range of respiration rates and stocks of the different source-specific OM. Then, for each OM stock, we proceeded as follows.

For leaf litter, we used over 1000 field measurements of leaf litter decay rates synthesized by Follstad Shah et al. (2017) (*see* Supporting Information Table S1). However, only a fraction of the leaf mass loss is directly respired. The literature reports a wide range for such fraction. For instance, Gulis and Suberkropp (2003) show that, on average, respiration accounted for 31% and 33% of carbon loss in maple and rhododendron leaves in a control reach, respectively, and for 56% and 43% in a nutrient-enriched reach. Elwood et al. (1981) estimated that microbial respiration accounted for between 33% (control reach) and 39% (high-level P-enriched reach) of the mass loss of red oak (*Quercus rubra* L.) leaves. However, Baldy and Gessner (1997) found that microbial respiration accounted for only 17% of alder (*Alnus glutinosa* [L.] *Gaertn.*) leaf mass loss in

Table 2. Estimated model parameters. Median values (0.95 quantile range) of the marginal posterior distribution. Last column reports the parameters averaged across sites. Last row reports $\bar{\theta}$: the weighted average of the temperature sensitivity parameters across sources, where the weight corresponds to the relative contribution of each source.

	Unit	Range	Walker Branch	Black Earth	East Canyon	Medina	Potomac	Average
$ER_{B,20}$	g O_2 m^{-2} d^{-1}	[0–10]	1.64 (1.28–1.97)	1.85 (1.12–2.38)	1.05 (0.63–1.38)	2.48 (2.21–2.71)	0.03 (0.00–0.19)	1.41
θ_B	—	[1.0–1.2]	1.002 (1.000–1.014)	1.014 (1.000–1.069)	1.068 (1.026–1.102)	1.036 (1.029–1.043)	1.076 (1.037–1.115)	1.04
β_{LF}	g O_2 m^{-2}	[0–1000]	114.33 (86.41–145.37)	305.42 (218.75–440.17)	209.15 (140.43–320.36)	22.78 (0.66–59.04)	11.20 (0.64–29.53)	132.58
θ_{LF}	—	[1.0–1.2]	1.005 (1.000–1.021)	1.047 (1.021–1.076)	1.009 (1.000–1.031)	1.071 (1.038–1.109)	1.075 (1.037–1.115)	1.04
τ_{LF}	d	[0–300]	149.14 (107.15–178.10)	62.20 (41.16–97.26)	186.87 (139.56–232.41)	168.99 (43.71–198.85)	126.71 (33.77–195.50)	138.78
β_{GPP}	—	[0–10]	0.62 (0.52–0.77)	1.00 (0.89–1.12)	0.80 (0.77–0.84)	0.44 (0.38–0.50)	0.44 (0.39–0.48)	0.66
θ_{GPP}	—	[1.0–1.2]	1.012 (1.000–1.043)	1.063 (1.043–1.085)	1.076 (1.069–1.083)	1.015 (1.002–1.031)	1.025 (1.016–1.034)	1.04
τ_{GPP}	d	[0–120]	6.63 (4.41–9.45)	0.09 (0.01–0.21)	0.09 (0.00–0.20)	0.14 (0.01–0.35)	1.57 (1.01–2.58)	1.70
β_Q	g O_2 m^{-2} d^{-1}	[0–10]	0.44 (0.23–0.82)	0.89 (0.52–1.90)	0.11 (0.06–0.22)	0.11 (0.08–0.16)	2.32 (2.00–2.62)	0.77
θ_Q	—	[1.0–1.2]	1.023 (1.001–1.061)	1.017 (1.001–1.053)	1.092 (1.057–1.131)	1.127 (1.098–1.158)	1.095 (1.081–1.111)	1.07
τ_Q	d	[0–120]	1.11 (0.70–1.76)	79.45 (50.02–110.57)	0.31 (0.02–1.49)	0.09 (0.01–0.19)	0.11 (0.01–0.25)	16.11
α_Q	—	[0–4]	1.12 (0.78–1.53)	2.57 (1.64–3.16)	1.76 (1.40–1.99)	1.10 (1.03–1.18)	0.59 (0.52–0.68)	1.43
ρ	—	[−1 to 1]	0.52 (0.50–0.54)	0.28 (0.24–0.32)	0.50 (0.47–0.51)	0.27 (0.25–0.30)	0.24 (0.21–0.27)	0.36
σ_ϵ	g O_2 m^{-2} d^{-1}	[0–3]	0.74 (0.71–0.77)	1.34 (1.29–1.39)	0.70 (0.68–0.72)	1.00 (0.97–1.03)	1.37 (1.33–1.42)	1.03
$\bar{\theta}$	—		1.01	1.03	1.05	1.03	1.05	

a stream with moderately high nutrients. Overall, previously published work suggests less than 50% of leaf litter breakdown is lost as respiration. However, nonrespiratory leaf mass losses, for example, via leached DOM or transfer to higher trophic levels, could be further respired with a short turnover time, and this additional contribution would be included with the leaf litter-associated respiration in our model. For this reason, we approximated that 50% of the decay rate contributes to respiration. We note that this approximation does not enter directly into the model and serves only to compare model results with literature values. Starting from the empirical values of leaf litter decay rate, we derived the probability distribution of empirical respiration rates using the above-mentioned approximation. Then, we calculated the corresponding range of the leaf litter stock necessary to support the respiration flux estimated by the model. Finally, we discuss how the estimated range of leaf litter stock compares with empirical values reported in the literature. Specific estimates of leaf litter standing crop for site Walker Branch (*see* Supporting Information Table S1) allowed a more direct comparison. In this case, starting from the empirical stock, we calculated the value of the respiration rate needed to support the respiration flux estimated by the model, and then we compared such value with the probability distribution derived from literature values.

In the case of the GPP-derived component, we calculated the ratio of average GPP-derived ER to average GPP (ER_{GPP}/GPP) and compared it to the distribution of autotrophic respiration fraction reported by Hall and Beaulieu (2013).

In our modeling framework, the OM related to discharge can have very different composition and origin: from DOC to POC, up to coarse OM material transported downstream to the stream reach. However, it is reasonable to assume that respired DOC represents a significant fraction of ER_Q. We therefore used a rationale similar to that introduced for ER_{LF} for discharge-derived ER and combined field measurements of DOC uptake velocities (summarized by Mineau et al. 2016; Supporting Information Table S1) with DOC concentrations. We retrieved DOC measurements for four out of five case studies (Supporting Information Table S1, data for the East Canyon site were not available). To compare model results, we needed to estimate the fraction of field measured uptake velocity that goes into respiration. In their review, Del Giorgio and Cole (1998) estimated that in riverine ecosystems bacterial growth efficiency (i.e., the fraction of carbon uptake that is not directly respired) ranges from 0.04 to 0.54. Accordingly, the complementary fraction (0.46–0.96) is respired. However, field measurements of DOC uptake account not only for bacterial uptake but also for other abiotic processes like sediment adsorption. Therefore, the fraction of total DOC uptake that is respired is generally lower than the respiration fraction of bacterial uptake. We thus deemed reasonable assuming around 50% of uptake is respired. The respiration associated with DOC can thus

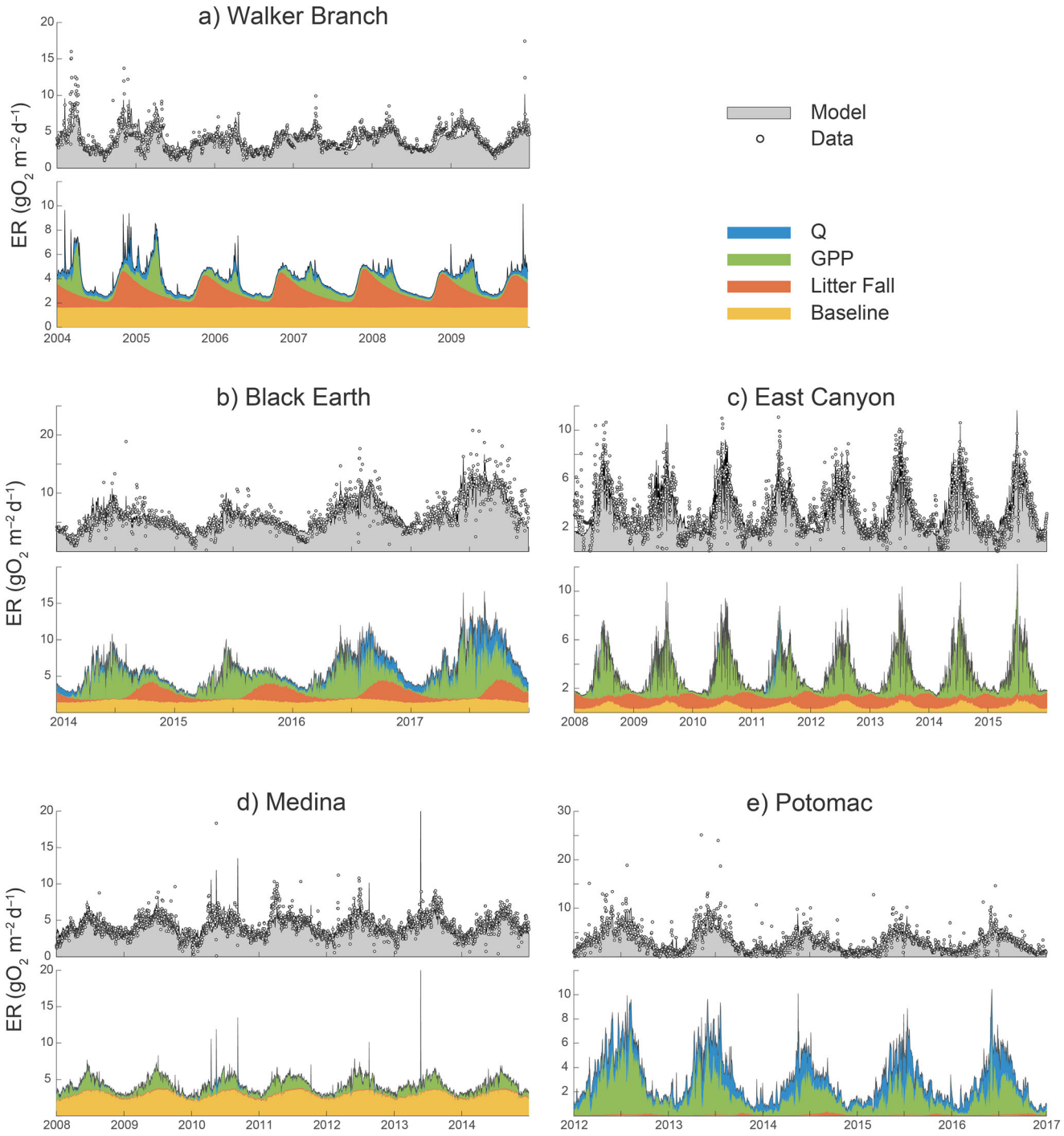

Fig. 2. Time series of estimated contributions to ER for the five case studies (**a**–**e**). In each panel, the top plot shows the comparison between the measured ER (circles) and the median value of the modeled ER (shaded area). Bottom plots report how the modeled ER is partitioned into the four contributions (shaded areas). Also in this case, median results are reported. For the probability distribution of each contribution, the reader is referred to the Supporting Information (Figs. S3, S7, S11, S15, and S19).

be computed as 50% of the product between DOC concentration and DOC uptake velocity. To compare model results with empirical values we proceeded as follows: from the DOC measured at the sites, we calculated the uptake velocity needed to support the respiration flux estimated by the model. Then, we compared such value with the empirical range of uptake velocities compiled from literature (Mineau et al. 2016).

We stress that model results are not affected by the assumptions of a respiratory fraction of 50% for both LF decay and DOC uptake, which are instead only used after the model application to provide an order of magnitude of the estimated fluxes against which model results are compared in order to check their plausibility.

Results

The developed OM respiration model was able to reproduce seasonal patterns of ER as well as fluctuations occurring at shorter time scales. Time series of the estimated contribution of the different OM stocks are shown in Fig. 2. This figure reports median results, for an appreciation of the uncertainty related to each component the reader is referred to the Supporting Information (Figs. S3, S7, S11, S15, and S19). In addition, the Supporting Information reports the comparison between the proxies used to approximate the OM inputs (namely, $Q(t)$, $\mathrm{GPP}(t)$, and $\mathrm{LF}(t)$) and the corresponding ER contributions (Figs. S4, S8, S12, S16, and S20). The average contribution of the four different OM stocks to the total ER is summarized in Fig. 3 and Supporting Information Table S2. General patterns suggest that leaf litter contributions to ER decrease with catchment size while GPP contributions generally increase. Although the Bayesian method used does not maximize the coefficient of determination, we reported the resulting values in Supporting Information Table S2 to provide an easily interpretable metric of the proportion of data variance explained by the model. R^2 ranged between 53% for Walker Branch and 74% for Black Earth and East Canyon.

Besides partitioning ER among OM stocks, the estimated parameters can provide predictions about the reactivity of the different OM stocks, their turnover time and their temperature sensitivity. Statistics of the parameter posterior distribution are reported in Table 2. The shape of the marginal distributions for each parameter and site is reported in the Supporting Information (Figs. S2, S6, S10, S14, and S18). Most of the marginal probability density functions converged to peaked distributions, except when a parameter was estimated to approach the zero physical boundary. This occurred when: (1) a contribution was estimated to be almost negligible and thus the parameter controlling the average respiration tended to zero ($\mathrm{ER}_{\mathrm{B},20}$ for Potomac, β_{LF} for Medina and Potomac); or (2) the lag between input and respiration was estimated to be very short (τ_{GPP} close to zero for Black Earth, East Canyon and Medina, τ_{Q} for Medina and Potomac). Moreover, nonpeaked distribution occurred when temperature sensitivity was estimated to be low and thus θ parameters tended to the unity lower boundary (all θ parameters for Walker Branch, θ_{B} for Black Earth, θ_{LF} for East Canyon).

The lag parameters τ reflect the average time elapsed between the inputs of OM and their respiration. The average τ_{LF} across sites was 138 d (Table 2), suggesting a long lag between leaf litter fall in the catchment (as measured by the proxy $\mathrm{LF}(t)$) and its respiration in the focus reach. For GPP-related respiration, the time lag was much shorter, around 1 d or shorter, suggesting that autochthonous OM was respired within one or few days, with the exception of Walker Branch site where the median τ_{GPP} was about 6.63 d. Also, respiration of OM stocks related to discharge had a very fast turnover,

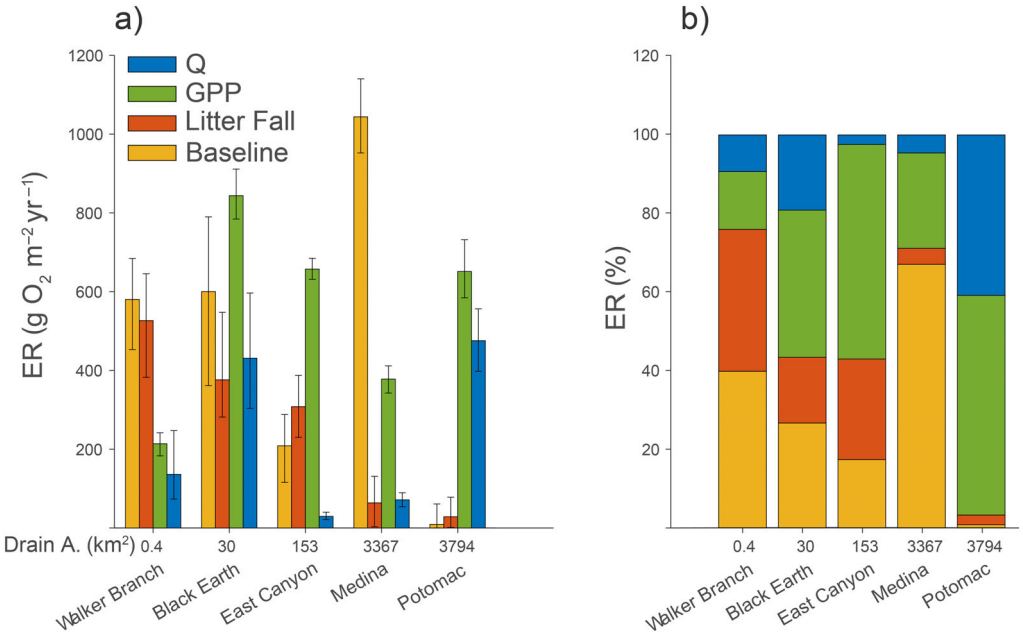

Fig. 3. Average annual ER contributions for the five case studies. (**a**) Median (bars) and 0.95 quantile range (error bars). (**b**) Same as (**a**) but normalized with respect to the total ER.

except for the site Black Earth, where median τ_Q was estimated to be about 79 d.

Compared to other parameters, temperature sensitivity of respiration exhibited less variability among the different OM stocks and among sites. The average (weighted according to the source contribution) temperature sensitivity $\overline{\theta}$ of the five sites was bracketed in the range (1.03–1.05), with the exception of the site Walker Branch, for which $\overline{\theta} = 1.01$ (Table 2).

Modeled ER compared well with available literature values. The contribution of leaf litter respiration to ER (with dimension [M L^{-2} T^{-1}]) can be thought of as the product between a respiration rate (T^{-1}) and a stock of leaf litter (M L^{-2}) in the streambed. However, as discussed above, the model cannot estimate the OM stock and respiration rate separately, only their product. Therefore, the slopes in Fig. 4a represent the paired magnitudes of respiration rate (expressed as d^{-1}) and average leaf litter stock (expressed as g C m^{-2}, assuming a 1 : 1 molar ratio between oxygen and carbon) that would result in the leaf litter-associated respiration estimated by the model. Such values are then compared with the probability distribution of leaf litter respiration rates from empirical studies (shaded area in Fig. 4a). For the most probable rates, the estimated average leaf litter stock ranges between about 2 g C m^{-2} for the Potomac up to about 200 g C m^{-2} for Walker Branch. We could gather direct observations on leaf litter dynamics only for the site Walker Branch. The observed average leaf litter stock of 38 g C m^{-2} (Supporting Information Table S1) corresponds to a respiration rate of around 0.012 d^{-1}, a value which sits close to the upper bound of the interquantile range of the empirical respiration rates (Fig. 4a).

We then compared the ratio between the estimated average GPP-related respiration and the average GPP, with the autotrophic respiration fraction (ARf) (Hall and Beaulieu 2013) (Fig. 4b). The ratio for the five case studies lies on the upper part of the ARf distribution.

Finally, Fig. 4c shows the analysis of the estimated discharge-related respiration. The analysis follows the same rationale of Fig. 4a showing the paired magnitudes of uptake velocity and average DOC concentration that would amount to the ER_Q estimated by the model (also in this case a 1 : 1 molar ratio between oxygen and carbon was assumed). The shaded area reports the range of uptake velocities derived from the ambient DOC uptake velocities corrected for biological availability (i.e., reactivity) as reported by Mineau et al. (2016). The uptake velocities corresponding to the empirical DOC concentrations (Supporting Information Table S1) lay within the empirical range except for the Medina site, which has the highest DOC concentration (3.6 g m^{-3}) but a relatively low estimate of ER_Q (Fig. 4c).

Discussion

Our study demonstrates that stream and river respiration regimes reflect the temporal dynamics of OM derived from distinct sources, namely leaf litter inputs, in situ autotrophic production (GPP), and flow-related OM inputs from the

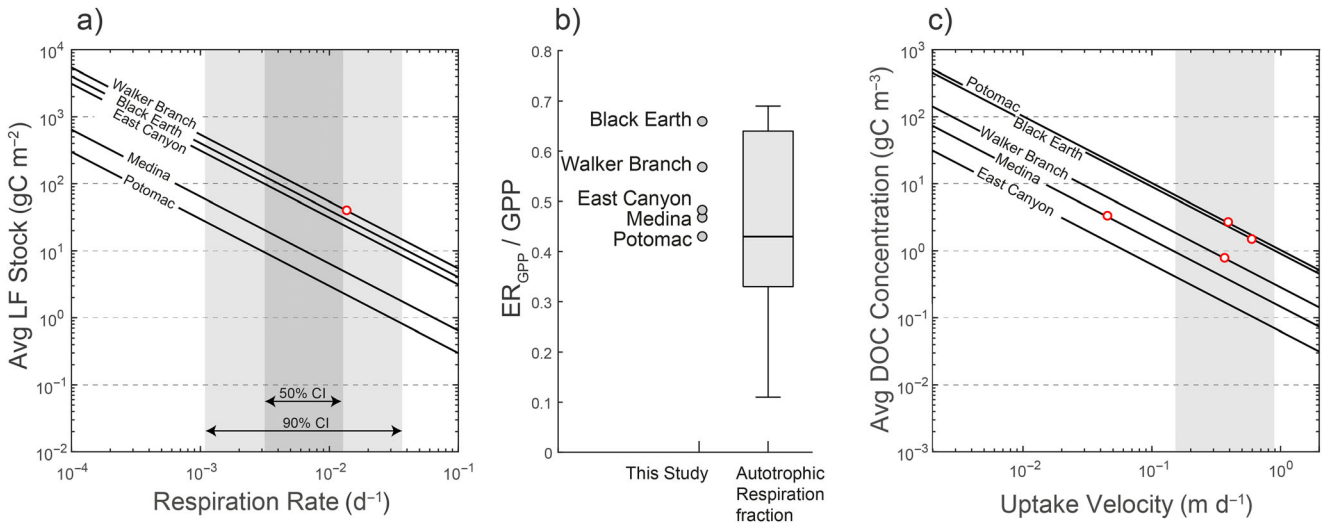

Fig. 4. Comparison between model estimates and literature values. (**a**) Leaf litter contribution: solid lines show the paired magnitudes of respiration rate and average stock of leaf litter that would result in the estimated leaf litter contribution to ER. Shaded areas show the 50% (darker gray) and 90% (lighter gray) quantile range of literature values of leaf litter respiration rates. The red circle shows the average leaf litter stock observed in Walker Branch (Supporting Information Table S1, assuming a 50% carbon fraction in AFDM; leaf litter stock data were not available for the other sites). (**b**) GPP contribution: ratio between average ER_{GPP} and average GPP (circles) compared to the distribution of autotrophic respiration fraction (box blot) (Hall and Beaulieu 2013). (**c**) Discharge contribution: solid lines show the paired magnitudes of DOC uptake velocity and average DOC concentration that would result in the estimated contribution of discharge-associated ER. The shaded area represents the range of uptake velocities retrieved from Mineau et al. (2016). Red circles show the observed average DOC concentration, when available (Supporting Information Table S1).

catchment. A combination of sediment OM and baseflow-associated OM delivery supported baseline ER after accounting for the more dynamic OM stocks contributing to ER. Using an inverse modeling approach that attributes ER regimes components to different OM sources, we explained a substantial fraction (range 53–74%) of variance in multi-year ER time series. We also showed that high-frequency, multi-year time-series data contain enough information to partition the contribution of OM derived from different sources to ER, and to quantify the lags between various OM inputs and their decomposition.

One important feature of our approach is that the use of forcing time series (litterfall, GPP, discharge, temperature) reduces the need for investigators to specify a priori the size and reactivity of OM stocks. Instead, estimates of these characteristics can be extracted from the joint dynamics of respiration and its drivers. The primary limitations of this approach are that (1) we do not obtain independent estimates of OM stock sizes and source-specific respiration rates, and (2) temporal covariation among proxies used for OM inputs and environmental variables could cause mis-attribution of respiration across OM compartments. For instance, in the case of correlation between temperature and discharge, typical of glacier-fed streams, the model could exchange respiration related to discharge with an enhanced temperature sensitivity for the baseline respiration, or vice versa. Correlation between GPP and temperature, or between discharge and litterfall, could generate similar mis-attributions. To alleviate this potential problem, it is advisable to gather information to better constrain the prior parameter distribution. Finally, the small autocorrelation in the model residuals (average $\rho = 0.36$, Table 2) suggests that there could be some processes regulating ER that are not accounted for by the model. While these limitations should caution against overconfidence in exact values derived from our model results, they should also provide new motivation, direction, and context for mechanistic studies that integrate measurements and models of OM storage, metabolism, and transport in streams (Webster and Meyer 1997; Duarte and Prairie 2005; Tank et al. 2010).

Respiration dynamics

Our modeling approach inferred patterns of respiration over time, among rivers, and across OM sources that agree with our current understanding of variation in the timing of OM delivery, the reactivity of different OM stocks (Marn-Spiotta et al. 2014; Lehmann and Kleber 2015), and their changing importance with river width. The contributions of OM derived from different sources to ER were generally within reasonable ranges given what is known about the range of OM stock sizes and respiration rates of different forms and sources of OM. For some sites and sources, these estimates are in good agreement; in other cases, our results suggest a need to better constrain parameters to reduce uncertainty in how respiration is partitioned among different OM stocks, as detailed in the following.

Leaf litter contribution to ER monotonically decreased with catchment size and channel width. This feature was expected because direct leaf litterfall per unit of streambed area decreases with stream width; and input from the upstream network attenuates going downstream because of the concurrent degradation (Vannote et al. 1980). For the five study sites our model predicted that average leaf litter standing stocks of 2 to 200 g C m^{-2} (Fig. 4a) were needed to maintain the estimated leaf litter contribution to ER. This range is comparable to results from field studies in temperate streams reporting leaf litter standing stocks of as low as 4 g of ash free dry mass (AFDM) m^{-2} (Sycamore Creek, Sonoran Desert, Wallace et al. 1999) and up to 450 g AFDM m^{-2} (deciduous forest streams in Portugal, Graça and Canhoto 2006). Direct observation in one of the study sites, Walker Branch, allowed a more refined assessment of the model results and confirmed that model estimates of leaf litter-related respiration for this site are reasonable. Lags between leaf litter and respiration ranged from 62 to 187 d, supporting the persistence of at least a fraction of the leaf litter-derived OM fueling ER in many sites. Walker Branch analyses allowed a further appraisal of the model estimates: temporal patterns of leaf litter-derived respiration (Fig. 2; Supporting Information Fig. S4) are in very good agreement with the annual pattern of leaf litter standing stock reported for the same site in fig. 1b of Suberkropp (1997), which peaks in November and maintains a residual stock throughout the summer.

Across study sites, the fraction of respiration related to autochthonous GPP aligned with the magnitude of mean GPP and was lowest in the smallest catchment (Walker Branch) and highest in the largest one (Potomac). Lags for GPP-supported respiration were short, consistent with the known high reactivity of autochthonous OM (Myklestad 1995; Descy et al. 2002; Guenet et al. 2010) and rapid turnover of newly fixed GPP (Hotchkiss and Hall Jr. 2015). The ratio of GPP-related respiration to GPP ranged from 0.43 to 0.68 and was similar, or slightly higher than the autotrophic respiration fraction estimated with other methods by Hall and Beaulieu (2013). It is important to mention that the analysis by Hall and Beaulieu (2013) refers to autotrophic respiration and closely associated heterotrophs; our model instead has a broader definition of GPP-derived respiration. Moreover, Hall and Beaulieu (2013) focused on a daily timescale, while our model accounted for possible longer delay between OM production and respiration. It was thus expected that our estimates could be biased toward higher values than those estimated by the autotrophic respiration fraction. Like most other approaches, our model does not allow us to differentiate respiration by autotrophs from heterotrophs, but future versions of our modeling framework could be developed to test these lingering unknowns in whole-stream carbon budgets.

Hydrologic drivers can affect ER through different pathways and mechanisms, and such variability was reflected also in our estimates of discharge-driven respiration across study sites. Walker Branch, Medina, and Potomac River had similar patterns with a short lag τ_Q and exponents α_Q in the range 0.6–1.12. The latter is in agreement with the power–law relationships typically found between DOC and discharge (Raymond and Saiers 2010; Fasching et al. 2014). The combination of these two parameters suggests that in these three sites discharge-related ER is dominated by respiration of labile DOC delivered to the stream during high-flow events (Demars 2019). Indeed, when comparing observations of DOC concentrations and empirical DOC uptake velocities, our model estimates agreed well for Walker Branch and Potomac (Fig. 4c). On the contrary, the high DOC concentration observed in Medina does not seem compatible with our estimates of discharge-related ER. These apparently contradictory results could be reconciled noting that, in our framework, the baseline respiration includes also the contribution of respiration of DOM transported during baseflow. Medina had a comparatively high baseline contribution that could account also for respiration of DOC. However, further empirical evidence on the site DOC dynamics and composition would be needed to confirm this interpretation. Also, East Canyon had a behavior similar to the three sites described above, although with a slightly higher α_Q. However, ER_Q had an overall a minimal contribution (2%) which could hamper a reliable parameter identification. Moreover, we could not retrieve direct observations of DOC concentration for this site. These two factors restrained us from further elaborate on this result. Black Earth Creek showed instead very different dynamics characterized by high α_Q and long lags τ_Q (*see* also Supporting Information Fig. S8). Such strong non-linear response suggests that only few large flow events led to an increased transport into the stream of OM characterized by low reactivity that could sustain, although with an overall small contribution (18%), the ER for long periods. Such behavior suggests a more POC-dominated response to flow events; however, also in this case further empirical evidence would be needed.

Baseline respiration has several potential OM-derived sources including respiration of wood and other coarse particulate organic material, fine particulates stored on the streambed and in hyporheic sediments, and respiration of DOM delivered under baseflow conditions. Without more information about these more temporally stable OM stocks, it is difficult to make predictions across sites. We did find that temporally-stable respiration made very different contributions across sites. Potomac had no baseline contribution. However, this is reasonable given that ER was very low in winter, and discharge related respiration contributed the most to this stream. In contrast to the Potomac case study, the other stream case studies had high baseline and low discharge contributions to ER.

We did not have any a priori expectation regarding the variation of temperature sensitivity parameters θ and we could not find a posteriori any systematic changes of such parameters, across both OM sources and sites. We note that some θ parameters were difficult to identify and the marginal posterior distribution tended toward the imposed lower boundary of 1 (i.e., no sensitivity to temperature). This occurred in two study sites for the baseline respiration temperature sensitivity (Walker Branch and Black Earth). A possible explanation is that we used streamflow water temperature; however, if a large fraction of the estimated baseline respiration occurs in the hyporheic zone, organisms therein experience a temperature signal more damped than the one of the water column (Wondzell 2011). This mismatch would be accommodated in the model by estimating an apparently lower temperature sensitivity. Therefore, θ_B close to one could cautiously be interpreted as a clue that the bulk on the baseline respiration occurs in deeper sediments rather than in the benthic surface and the water column. Moreover, we found that all θ parameters tended toward 1 for Walker Branch. In this regard, it should be noted that this site is the only one that showed an ER inversely correlated with temperature, with higher respiration during winter. Therefore, irrespective of the proposed model details, any kind of regression model would likely tend to minimize a positive effect of temperature on ER. A more informative and site-specific prior distribution for this parameter would be needed to better differentiate the role of timing of OM stocks and temperature in shaping the seasonal patterns of ER.

Time-series approaches and the mechanistic understanding of river network respiration

Leveraging long-term and high-frequency measurements of dissolved oxygen, temperature, and remotely sensed ancillary variables can provide useful information on reach-scale OM mass balance and respiration dynamics in streams and rivers, and can thus constitute an effective substitute or companion to traditional experimental and field approaches to study OM dynamics. For the Walker Branch case study site, we showed that concomitant availability of both long-term time-series and classical OM budget and experimental studies allowed a more in-depth assessment of the reliability of model results and its potential limitations. Therefore, the modeling and data collection approaches should be seen as complementary tools that can synergistically improve our ability to understand the functioning of stream ecosystems. Further development of the model should thus prioritize (1) expanding field data collection in sites that already have long time series of metabolism and/or (2) deploying high-frequency sensors in reaches where OM budgets already exist.

Our modeling framework focuses on a single reach and subsumes the effects of transport and transformation processes occurring in the upstream catchment in the τ lag parameters. We thus adopted the traditional "field of view" of stream ecosystem research: the reach. However, an emerging consensus is arising in the scientific community about the need to adopt

a network perspective to fully appreciate and predict ecosystem processes (Koenig et al. 2019; Segatto et al. 2021; Wollheim et al. 2022) and biogeochemical fluxes (Raymond et al. 2016; Bertuzzo et al. 2017; Helton et al. 2018). A possible pathway to model development is thus the integration of a more mechanistic description of OM inputs and transport along the river network. A network-scale framework should couple a hydrologic model to reconstruct lateral flows with a hydraulic model to simulate flow conditions and related transport. Moreover, it could exploit distributed information, possibly acquired also through remote sensing, about land cover and land use to predict inputs and fates of DOM (*see* Grandi and Bertuzzo 2022) and leaf litter along the network. The integration of these modeling components would better constrain the estimation of OM stocks (e.g., for leaf litter and DOC) and separate it from that of the corresponding respiration rate. Indeed, the inability to separate these two factors is one of the main limitations of the current model formulation. To facilitate this kind of study, it is important to stress the need to design experimental campaigns with a network "field of view," for instance with the deployment of several measurement stations nested within the same catchment (*see* Ulseth et al. 2018; Segatto et al. 2020).

One critical need in aquatic ecology is to improve our understanding of the links between ecosystem processes and biota (Marcarelli et al. 2011; Ruegg et al. 2021). Because our approach converts metabolic fluxes to dynamic stocks, it provides a new tool that can link the phenology of biota to metabolic regimes, and provide meaningful proxies for dynamics of OM resource availability for population, community, and food web research. Because our approach infers processes from dynamic time series, its outputs could be used to forecast how respiration regimes will respond to changing environmental drivers such as increasing temperature (Kaushal et al. 2010; Song et al. 2018), modified flow regimes, and changes in OM and nutrient availability (Rosemond et al. 2015; Kominoski et al. 2018). The magnitude and phenology of stream metabolism will be determined by the interactions between OM, biota phenology and global changes in temperature and precipitation. Hydrologic- and temperature-driven environmental changes and disturbance events can determine the quantity, quality, and phenology of basal resources (e.g., detrital or algal OM) as well as their use by microbes (Baines et al. 2000; Erlandsson et al. 2008) and overall effects on stream autotrophic and heterotrophic processes (Kominoski and Rosemond 2012; Rosemond et al. 2015; Bernhardt et al. 2018).

What controls respiration rates in ecosystems? What is the fate of algal and terrestrial-derived OM as it travels through river networks and food webs? How might future environmental changes alter the carbon budgets and respiration regimes of streams, rivers, and river networks? As we find ourselves in an era of ecology supported by in situ sensors, remote sensing and other large datasets, mechanistic modeling frameworks to characterize and predict whole-ecosystem processes will play a critical role in knowledge advancement and ecosystem management. Our model characterizing the respiration regimes of five case study sites was validated by existing datasets, provided new insights into the reactivity and respiration of different OM stocks across streams and rivers, and offers numerous opportunities to advance ecosystem science in the future.

Data Availability Statement

No new data were generated for this study. Data used for all sites except Walker Branch are available at https://data.streampulse.org. Preprocessed input data and model codes are available at the following public repository: https://doi.org/10.5281/zenodo.7056615

References

Acuña, V., A. Wolf, U. Uehlinger, and K. Tockner. 2008. Temperature dependence of stream benthic respiration in an Alpine river network under global warming. Freshw. Biol. **53**: 2076–2088. doi:10.1111/j.1365-2427.2008.02028.x

Appling, A. P., and others. 2018. The metabolic regimes of 356 rivers in the United States. Sci. Data **5**: 180292. doi:10.1038/sdata.2018.292

Baines, S. B., K. E. Webster, T. K. Kratz, S. R. Carpenter, and J. J. Magnuson. 2000. Synchronous behavior of temperature, calcium, and chlorophyll in lakes of northern Wisconsin. Ecology **81**: 815–825. doi:10.2307/177379

Baldy, V., and M. O. Gessner. 1997. Towards a budget of leaf litter decomposition in a first-order woodland stream. C. R. Acad. Sci. Ser. III Sci. Vie **320**: 747–758. doi:10.1016/S0764-4469(97)84824-X

Battin, T. J., L. A. Kaplan, S. Findlay, C. S. Hopkinson, E. Marti, A. I. Packman, J. D. Newbold, and F. Sabater. 2008. Biophysical controls on organic carbon fluxes in fluvial networks. Nat. Geosci. **1**: 95–100. doi:10.1038/ngeo101

Bernhardt, E. S., and others. 2018. The metabolic regimes of flowing waters. Limnol. Oceanogr. **63**: S99–S118. doi:10.1002/lno.10726

Bertuzzo, E., A. M. Helton, R. O. Hall Jr., and T. J. Battin. 2017. Scaling of dissolved organic carbon removal in river networks. Adv. Water Resour. **110**: 136–146. doi:10.1016/j.advwatres.2017.10.009

Cohen, M. J., M. J. Kurz, J. B. Heffernan, J. B. Martin, R. L. Douglass, C. R. Foster, and R. G. Thomas. 2013. Diel phosphorus variation and the stoichiometry of ecosystem metabolism in a large spring-fed river. Ecol. Monogr. **83**: 155–176. doi:10.1890/12-1497.1

Del Giorgio, P. A., and J. J. Cole. 1998. Bacterial growth efficiency in natural aquatic systems. Ann. Rev. Ecol. Syst. **29**: 503–541. doi:10.1146/annurev.ecolsys.29.1.503

Demars, B. O. 2019. Hydrological pulses and burning of dissolved organic carbon by stream respiration. Limnol. Oceanogr. **64**: 406–421. doi:10.1002/lno.11048

Descy, J.-P., B. Leporcq, L. Viroux, C. François, and P. Servais. 2002. Phytoplankton production, exudation and bacterial reassimilation in the River Meuse (Belgium). J. Plankton Res. **24**: 161–166. doi:10.1093/plankt/24.3.161

Duarte, C. M., and Y. T. Prairie. 2005. Prevalence of heterotrophy and atmospheric CO_2 emissions from aquatic ecosystems. Ecosystems **8**: 862–870. doi:10.1007/s10021-005-0177-4

Eklundh, L., and P. Jönsson. 2015. TIMESAT: A software package for time-series processing and assessment of vegetation dynamics, p. 141–158. *In* Remote sensing time series. Springer.

Elwood, J. W., J. D. Newbold, A. F. Trimble, and R. W. Stark. 1981. The limiting role of phosphorus in a woodland stream ecosystem: Effects of P enrichment on leaf decomposition and primary producers. Ecology **62**: 146–158. doi:10.2307/1936678

Erlandsson, M., I. Buffam, J. Fölster, H. Laudon, J. Temnerud, G. A. Weyhenmeyer, and K. Bishop. 2008. Thirty-five years of synchrony in the organic matter concentrations of Swedish rivers explained by variation in flow and sulphate. Glob. Chang. Biol. **14**: 1191–1198. doi:10.1111/j.1365-2486.2008.01551.x

Fasching, C., B. Behounek, G. A. Singer, and T. J. Battin. 2014. Microbial degradation of terrigenous dissolved organic matter and potential consequences for carbon cycling in brown-water streams. Sci. Rep. **4**: 4981. doi:10.1038/srep04981

Fasching, C., A. J. Ulseth, J. Schelker, G. Steniczka, and T. J. Battin. 2016. Hydrology controls dissolved organic matter export and composition in an Alpine stream and its hyporheic zone. Limnol. Oceanogr. **61**: 558–571. doi:10.1002/lno.10232

Follstad Shah, J. J., and others. 2017. Global synthesis of the temperature sensitivity of leaf litter breakdown in streams and rivers. Glob. Chang. Biol. **23**: 3064–3075. doi:10.1111/gcb.13609

Gillooly, J. F., J. H. Brown, G. B. West, V. M. Savage, and E. L. Charnov. 2001. Effects of size and temperature on metabolic rate. Science **293**: 2248–2251. doi:10.1126/science.1061967

Graça, M. A., and C. Canhoto. 2006. Leaf litter processing in low order streams. Limnetica **25**: 1–10. doi:10.23818/limn.25.01

Grace, M. R., D. P. Giling, S. Hladyz, V. Caron, R. M. Thompson, and R. Mac Nally. 2015. Fast processing of diel oxygen curves: Estimating stream metabolism with BASE (BAyesian Single-station Estimation). Limnol. Oceanogr. Methods **13**: 103–114. doi:10.1002/lom.10011

Grandi, G., and E. Bertuzzo. 2022. Catchment dissolved organic carbon transport: A modeling approach combining water travel times and reactivity continuum. Water Resour. Res. **58**: e2021WR031275. doi:10.1029/2021WR031275

Guenet, B., M. Danger, L. Abbadie, and G. Lacroix. 2010. Priming effect: Bridging the gap between terrestrial and aquatic ecology. Ecology **91**: 2850–2861. doi:10.1890/09-1968.1

Gulis, V., and K. Suberkropp. 2003. Leaf litter decomposition and microbial activity in nutrient-enriched and unaltered reaches of a headwater stream. Freshw. Biol. **48**: 123–134. doi:10.1046/j.1365-2427.2003.00985.x

Hall, R. O., and J. J. Beaulieu. 2013. Estimating autotrophic respiration in streams using daily metabolism data. Freshw. Sci. **32**: 507–516. doi:10.1899/12-147.1

Heffernan, J. B., and M. J. Cohen. 2010. Direct and indirect coupling of primary production and diel nitrate dynamics in a subtropical spring-fed river. Limnol. Oceanogr. **55**: 677–688. doi:10.4319/lo.2010.55.2.0677

Helton, A. M., R. O. Hall Jr., and E. Bertuzzo. 2018. How network structure can affect nitrogen removal by streams. Freshw. Biol. **63**: 128–140. doi:10.1111/fwb.12990

Holtgrieve, G. W., D. E. Schindler, T. A. Branch, and Z. T. A'mar. 2010. Simultaneous quantification of aquatic ecosystem metabolism and reaeration using a Bayesian statistical model of oxygen dynamics. Limnol. Oceanogr. **55**: 1047–1063. doi:10.4319/lo.2010.55.3.1047

Hotchkiss, E. R., and R. O. Hall Jr. 2015. Whole-stream ^{13}C tracer addition reveals distinct fates of newly fixed carbon. Ecology **96**: 403–416. doi:10.1890/14-0631.1

Hotchkiss, E., R. Hall Jr., R. Sponseller, D. Butman, J. Klaminder, H. Laudon, M. Rosvall, and J. Karlsson. 2015. Sources of and processes controlling CO_2 emissions change with the size of streams and rivers. Nat. Geosci. **8**: 696–699. doi:10.1038/ngeo2507

Jönsson, P., and L. Eklundh. 2004. TIMESAT a program for analyzing time-series of satellite sensor data. Comput. Geosci. **30**: 833–845. doi:10.1007/978-3-319-15967-6_7

Kaushal, S. S., and others. 2010. Rising stream and river temperatures in the United States. Front. Ecol. Environ. **8**: 461–466. doi:10.1890/090037

Koenig, L. E., A. M. Helton, P. Savoy, E. Bertuzzo, J. B. Heffernan, R. O. Hall Jr., and E. S. Bernhardt. 2019. Emergent productivity regimes of river networks. Limnol. Oceanogr. Lett. **4**: 173–181. doi:10.1002/lol2.10115

Kominoski, J. S., and A. D. Rosemond. 2012. Conservation from the bottom up: Forecasting effects of global change on dynamics of organic matter and management needs for river networks. Freshw. Sci. **31**: 51–68. doi:10.1899/10-160.1

Kominoski, J. S., A. D. Rosemond, J. P. Benstead, V. Gulis, and D. W. Manning. 2018. Experimental nitrogen and phosphorus additions increase rates of stream ecosystem respiration and carbon loss. Limnol. Oceanogr. **63**: 22–36. doi:10.1002/lno.10610

Lehmann, J., and M. Kleber. 2015. The contentious nature of soil organic matter. Nature **528**: 60–68. doi:10.1038/nature16069

Leopold, L., and T. Maddock. 1953. The hydraulic geometry of stream channels and some physiographic implications. U.S.

Government Printing Office, Washington, D.C. Report Geological Survey Professional Paper 252. doi:10.3133/pp252

Mallin, M., V. Johnson, S. Ensign, and T. MacPherson. 2006. Factors contributing to hypoxia in rivers, lakes, and streams. Limnol. Oceanogr. **51**: 690–701. doi:10.4319/lo.2006.51.1_part_2.0690

Marcarelli, A. M., C. V. Baxter, M. M. Mineau, and R. O. Hall Jr. 2011. Quantity and quality: Unifying food web and ecosystem perspectives on the role of resource subsidies in freshwaters. Ecology **92**: 1215–1225. doi:10.1890/10-2240.1

Marn-Spiotta, E., K. Gruley, J. Crawford, E. Atkinson, J. Miesel, S. Greene, C. Cardona-Correa, and R. Spencer. 2014. Paradigm shifts in soil organic matter research affect interpretations of aquatic carbon cycling: Transcending disciplinary and ecosystem boundaries. Biogeochemistry **117**: 279–297. doi:10.1007/s10533-013-9949-7

Mineau, M. M., and others. 2016. Dissolved organic carbon uptake in streams: A review and assessment of reach-scale measurements. J. Geophys. Res. Biogeosci. **121**: 2019–2029. doi:10.1002/2015JG003204

Mulholland, P. J., and others. 2008. Stream denitrification across biomes and its response to anthropogenic nitrate loading. Nature **452**: 202–205. doi:10.1038/nature06686

Myklestad, S. M. 1995. Release of extracellular products by phytoplankton with special emphasis on polysaccharides. Sci. Total Environ. **165**: 155–164. doi:10.1016/0048-9697(95)04549-G

Myneni, R., Y. Knyazikhin, and T. Park. 2015. MCD15A2H MODIS/Terra+ aqua leaf area index/FPAR 8-day L4 global 500 m SIN grid V006. NASA EOSDIS Land Processes DAAC. doi:10.5067/MODIS/MOD15A2H.006

O'Donnell, B., and E. R. Hotchkiss. 2019. Coupling concentration- and process-discharge relationships integrates water chemistry and metabolism in streams. Water Resour. Res. **55**: 10179–10190. doi:10.1029/2019WR025025

Prairie, Y., and J. Cole. 2009. Carbon, unifying currency, p. 743–746. *In* G. Likens [ed.], Encylopedia of inland waters. Academic Press. doi:10.1016/B978-012370626-3.00107-1

R Core Team. 2017. R: A language and environment for statistical computing. R Foundation for Statistical Computing.

Raymond, P. A., and J. E. Saiers. 2010. Event controlled DOC export from forested watersheds. Biogeochemistry **100**: 197–209. doi:10.1007/sl0533-010-9416-7

Raymond, P. A., J. E. Saiers, and W. V. Sobczak. 2016. Hydrological and biogeochemical controls on watershed dissolved organic matter transport: Pulse-shunt concept. Ecology **97**: 5–16. doi:10.1890/14-1684.1

Roberts, B. J., and P. J. Mulholland. 2007. In-stream biotic control on nutrient biogeochemistry in a forested stream, West Fork of Walker Branch. J. Geophys. Res. Biogeo. **112**: G04002. doi:10.1029/2007JG000422

Roberts, B. J., P. J. Mulholland, and W. R. Hill. 2007. Multiple scales of temporal variability in ecosystem metabolism rates: Results from 2 years of continuous monitoring in a forested headwater stream. Ecosystems **10**: 588–606. doi:10.1007/s10021-007-9059-2

Rode, M., and others. 2016. Sensors in the stream: The high-frequency wave of the present. Environ. Sci. Technol. **50**: 10297–10307. doi:10.1021/acs.est.6b02155

Rosemond, A. D., J. P. Benstead, P. M. Bumpers, V. Gulis, J. S. Kominoski, D. W. Manning, K. Suberkropp, and J. B. Wallace. 2015. Experimental nutrient additions accelerate terrestrial carbon loss from stream ecosystems. Science **347**: 1142–1145. doi:10.1126/science.aaa1958

Ruegg, J., and others. 2021. Thinking like a consumer: Linking aquatic basal metabolism and consumer dynamics. Limnol. Oceanogr. Lett. **6**: 1–17. doi:10.1002/lol2.10172

Savoy, P., A. P. Appling, J. B. Heffernan, E. G. Stets, J. S. Read, J. W. Harvey, and E. S. Bernhardt. 2019. Metabolic rhythms in flowing waters: An approach for classifying river productivity regimes. Limnol. Oceanogr. **64**: 1835–1851. doi:10.1002/lno.11154

Segatto, P. L., T. J. Battin, and E. Bertuzzo. 2020. Modeling the coupled dynamics of stream metabolism and microbial biomass. Limnol. Oceanogr. **65**: 1573–1593. doi:10.1002/lno.11407

Segatto, P. L., T. J. Battin, and E. Bertuzzo. 2021. The metabolic regimes at the scale of an entire stream network unveiled through sensor data and machine learning. Ecosystems **24**: 1–18. doi:10.1007/s10021-021-00618-8

Song, C., and others. 2018. Continental-scale decrease in net primary productivity in streams due to climate warming. Nat. Geosci. **11**: 415–420. doi:10.1038/s41561-018-0125-5

Stanley, E., N. Casson, S. Christel, J. Crawford, L. Loken, and S. Oliver. 2016. The ecology of methane in streams and rivers: Patterns, controls, and global significance. Ecol. Monogr. **86**: 146–171. doi:10.1890/15-1027

Suberkropp, K. 1997. Annual production of leaf-decaying fungi in a woodland stream. Freshw. Biol. **38**: 169–178. doi:10.1046/j.1365-2427.1997.00203.x

Tank, J. L., E. J. Rosi-Marshall, N. A. Griffiths, S. A. Entrekin, and M. L. Stephen. 2010. A review of allochthonous organic matter dynamics and metabolism in streams. J. North Am. Benthol. Soc. **29**: 118–146. doi:10.1899/08-170.1

Ter Braak, C. J., and J. A. Vrugt. 2008. Differential evolution Markov chain with snooker updater and fewer chains. Stat. Comput. **18**: 435–446. doi:10.1007/s11222-008-9104-9

Ulseth, A. J., E. Bertuzzo, G. A. Singer, J. Schelker, and T. J. Battin. 2018. Climate-induced changes in spring snowmelt impact ecosystem metabolism and carbon fluxes in an alpine stream network. Ecosystems **21**: 373–390. doi:10.1007/s10021-017-0155-7

Vannote, R. L., G. W. Minshall, K. W. Cummins, J. R. Sedell, and C. E. Cushing. 1980. The river continuum concept. Can. J. Fish. Aquat. Sci. **37**: 130–137. doi:10.1139/f80-017

Wallace, J. B., S. Eggert, J. L. Meyer, and J. Webster. 1999. Effects of resource limitation on a detrital-based ecosystem. Ecol. Monogr. **69**: 409–442 doi:10.1890/0012-9615(1999)069[0409:EORLOA]2.0.CO;2

Webster, J., and J. L. Meyer. 1997. Organic matter budgets for streams: A synthesis. J. North Am. Benthol. Soc. **16**: 141–161. doi:10.2307/1468247

Williams, P., and P. A. del Giorgio. 2005. Respiration in aquatic ecosystems: History and background, p. 1–17. *In* Respiration in aquatic ecosystems. Oxford Univ. Press. doi:10.1093/acprof:oso/9780198527084.003.0001

Wollheim, W. M., T. K. Harms, A. L. Robison, L. E. Koenig, A. M. Helton, C. Song, W. B. Bowden, and J. C. Finlay. 2022. Superlinear scaling of riverine biogeochemical function with watershed size. Nat. Commun. **13**: 1–9. doi:10.1038/s41467-022-28630-z

Wondzell, S. M. 2011. The role of the hyporheic zone across stream networks. Hydrol. Process. **25**: 3525–3532. doi:10.1002/hyp.8119

Wood, S. 2006. Generalized additive models: An introduction with R. *In* Texts in statistical science. Chapman & Hall. doi:10.1201/9781315370279

Acknowledgments

The authors would like to thank two anonymous Reviewers, the Associate Editor, and the Editor-in-Chief for their insightful and constructive comments. This work was initiated at the Heterotrophic Regimes workshop in Ovronnaz, Switzerland. We thank Tom Battin and Amber Ulseth for helping organize the workshop, and workshop participants for useful feedback on early conceptions of this model. Metabolism, temperature, and flow data for Walker Branch were provided by Brian Roberts and Natalie Griffiths and funded by the U.S. Department of Energy, Office of Science, Biological and Environmental Research Program. The authors acknowledge Patrick Mulholland and Brian Roberts for conducting the original Walker Branch study that serves as the foundation for much of our current work characterizing multi-annual stream metabolism dynamics. This project was supported by the Respiration Regimes in River Networks Workshop (NSF DEB #1832012), and the StreamPULSE project (www.streampulse.org; NSF DEB# 1442439). Daniel von Schiller is a Serra Hunter Fellow and was additionally supported by project Alter-C (PID2020-114024GB-C31) funded by MCIN/AEI/10.13039/501100011033. Alba Argerich was supported by USDA NIFA McIntire-Stennis Project #MO-MCNR0008. This is contribution #1484 from the Institute of Environment at Florida International University.

Conflict of Interest

None declared.

Submitted 14 April 2021
Revised 05 November 2021
Accepted 05 August 2022

Associate editor: K. David Hambright